1

Introduction to Untethered Miniature Soft Robots

1.1 Introduction

Miniature soft robots with inherent compliance could exhibit dynamic interaction with the real world [1, 2]. These controllable microdevices attracted growing attention because of their promises in a wide spectrum of applications, e.g. biomimetic study, environmental monitoring, precision medicine, as well as minimally invasive surgery [3, 4]. With a proper design of miniaturized structure and selection of material, the actuation and locomotion of miniature soft robots in tortuous and unstructured environments such as artificial vascular networks and animal tissues have been verified [5–8]. Advanced control techniques of physical fields allow us to elaborately tune the transformation of the robots, subsequently resulting in the generation of a variety of locomotion modes inspired by their natural counterparts, e.g. earthworm, inchworm, midge larvae, starfish larvae, bacteria, as well as jellyfish [9–14].

Various functional polymers have been introduced to endow robotic structures with intelligent properties, including self-healing property [15–17], degradability or stimuli-responsive deformation [18–21]. Due to the limited onboard space, conventional control units or driven parts can be hardly integrated into the miniature soft robots. In this respect, diverse stimuli-responsive materials (e.g. liquid crystal elastomers [LCE], shape memory polymers [SMP], and hydrogels) have been adopted for the construction of micromachines, so that they can present controllable deformation under external stimuli. In addition, to ensure the service life of soft robots, such as avoiding the influence of cracks caused by sharp parts in the physical environment or fatigue damages induced by multiple cycles of large deformations, self-healing polymers based on noncovalent interaction mechanisms or dynamic covalent networks have been proposed. Biomedical application is one of the most important development directions of miniature soft robots. The *in vivo* environments usually require the biodegradability or biocompatibility of robotic materials such as gelatin methacryloyl (GelMA) as well as zwitterionic materials [22, 23]. For instance, miniature soft machines have been applied for targeted cell delivery. The machines that load cells should be biocompatible to facilitate the adhesion and growth of therapeutic cells. Moreover, for robotic structures that can be hardly retrieved, they should

Untethered Miniature Soft Robots: Materials, Fabrications, and Applications, First Edition.
Li Zhang, Jiachen Zhang, Neng Xia, and Yue Dong.

be biodegradable to avoid the adverse effect of long-term accumulation. It is worth noting that sophisticated application scenarios may bring high requirements for the adaptability and versatility of a robotic system, which are often difficult to meet by robotic structures made of single-component materials difficult to meet. Therefore, the seamless integration of multiple functional modules or material compositions in the robotic system becomes pivotal, albeit a challenge [24, 25].

1.2 Working Mechanisms of Untethered Soft Robots

1.2.1 Magnetic Actuation

Soft robots actuated by external magnetic field have been intensively investigated due to their operation capability in large and enclosed workspaces, e.g. human body, and their great potential in minimally invasive surgery [26]. Magnetic field forces and torques could be used for the actuation of magnetic small-scale robots based on the interaction between the magnetic properties of the robot and the externally exerted magnetic fields (Figure 1.1a,b) [36, 37]. Assuming that there is no current

Figure 1.1 Working mechanisms of untethered soft robots. (a,b) Magnetic actuation [27, 28]. (a) A hexapod soft structure with programmable ferromagnetic domains was fabricated by direct ink writing (DIW) printing technique. The 2D–3D morphological transformation is realized under the action of magnetic torque. Source: Kim et al. [27]/Reproduced from Springer Nature. (b) A microneedle robot with a magnetic base navigates over obstacles and penetrates the wall of the small intestine under the control of permanent magnets. Source: Zhang et al. [28]/John Wiley &Sons. (c,d) Acoustic actuation [11, 29]. (c) Ultrasonic-powered microrobots inspired by starfish larvae. Under ultrasonic stimulation, the cilia array in the robot body produces a swinging motion, which in turn induces complex vortices flows. Source: Dillinger et al. [11]/Reproduced from Springer Nature/CC BY 4.0. (d) Ultrasound-actuated structures with arrays of bubbles. Under ultrasonic stimulation, the bubbles resonate and meanwhile form a thrust force acting on the surface of the structure. Source: Adapted from Qiu et al. [29]. (e,f) Light actuation [9, 30]. (e) The photo-responsive liquid crystal elastomer (LCE) generates oscillatory behavior under the stimulation of two mutually perpendicular laser beams, as well as the photothermal distribution on the surface of the LCE structure. Source: Deng et al. [30]/Reproduced from John Wiley & Sons, Inc./CC BY 4.0. (f) LCE-based soft robot driven by dynamic light field. The beam distribution in the space is adjusted in real time through a digital micromirror device (DMD), and then the deformation control of the soft robot is realized. Source: Palagi et al. [9]/Reproduced from Springer Nature. (g) Propulsion driven by Marangoni effect. A rove beetle-inspired hydrogel rotor achieves efficient rotation and energy transfer by consuming hexafluoroisopropanol (HFIP fuel). Source: Wu et al. [31]/Springer Nature/CC BY 4.0/Public domain. (h) Thermal actuation. The self-propelled rolling of a robot with a bilayer structure (ferroelectric polyvinylidene fluoride (PVDF) and polydopamine-modified reduced graphene oxide-carbon nanotube (PDG-CNT)) was realized via a mechano-thermal feedback loop. Source: Wang et al. [32]/Springer Nature/CC BY 4.0/Public domain. (i) Deformation driven by humidity stimuli. Source: Adapted from Dong et al. [33]. (j) Chemical actuation. Source: Hu et al. [34]/John Wiley & Sons. (k) Biohybrid actuation. Source: Wang et al. [35]/American Association for the Advancement of Science.

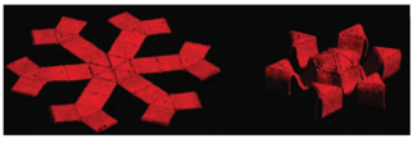

(a)

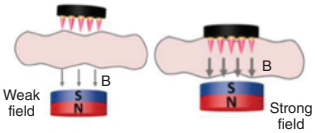

(b)

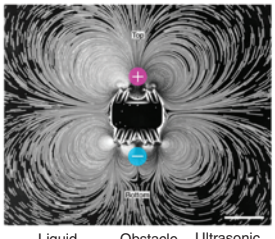

(c)

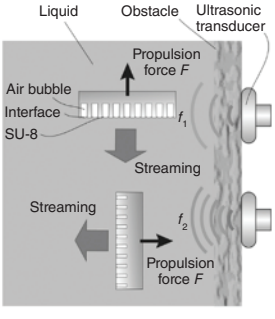

(d)

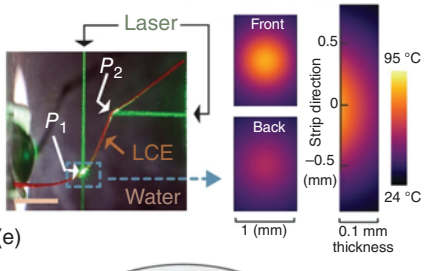

(e)

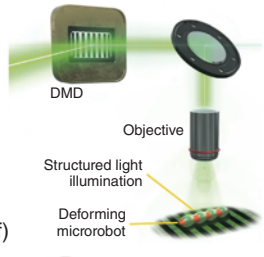

(f)

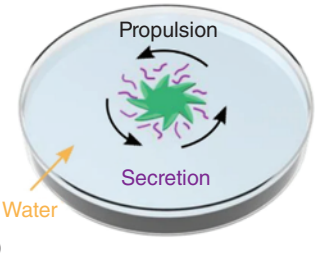

(g)

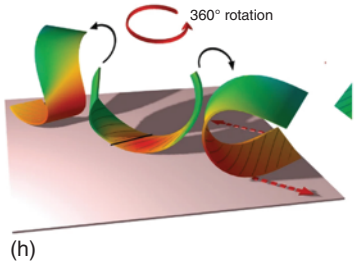

(h)

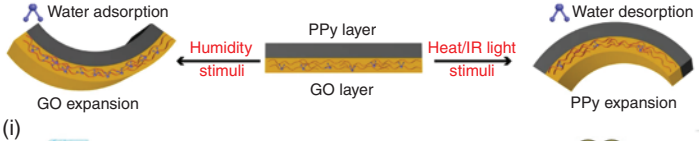

(i)

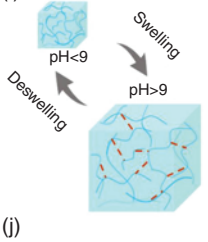

(j)

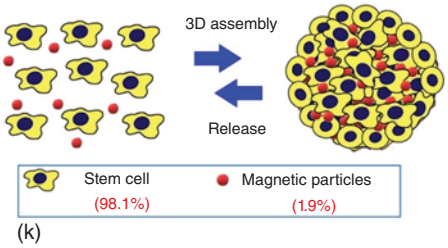

(k)

in the workspace, according to Maxwell's equations, it can be derived that the static magnetic field satisfies Eq. (1.1) [38]:

$$\nabla \cdot \boldsymbol{B} = 0 \nabla \times \boldsymbol{B} = 0 \tag{1.1}$$

where $\boldsymbol{B} = [B_x, B_y, B_z]$ represents the applied magnetic field, whose gradient matrix is traceless and symmetric.

The magnetic force (f) and torque (τ) applied to a magnetic device that are induced by a nonuniform field and the misalignment of directions of magnetic field and magnetization, respectively, can be calculated as Eq. (1.2) and Eq. (1.3):

$$\tau = \boldsymbol{m} \times \boldsymbol{B} = \begin{bmatrix} 0 & B_z & -B_y \\ -B_z & 0 & B_x \\ B_y & -B_x & 0 \end{bmatrix} \begin{bmatrix} m_x \\ m_y \\ m_z \end{bmatrix} \tag{1.2}$$

$$f = (m \cdot \nabla)B = \begin{bmatrix} \frac{\partial B_x}{\partial x} & \frac{\partial B_x}{\partial y} & \frac{\partial B_x}{\partial z} \\ \frac{\partial B_x}{\partial y} & \frac{\partial B_y}{\partial y} & \frac{\partial B_y}{\partial z} \\ \frac{\partial B_x}{\partial z} & \frac{\partial B_y}{\partial z} & -\left(\frac{\partial B_x}{\partial x} + \frac{\partial B_y}{\partial y}\right) \end{bmatrix} \begin{bmatrix} m_x \\ m_y \\ m_z \end{bmatrix} \tag{1.3}$$

The programmable parameters of magnetic field include the direction, amplitude, and gradient. Thanks to the high temporal resolution control and the capability of deep tissue penetration, multimodal locomotion including biomimetic modes on various terrains, sophisticated functionalities, and shape-morphing behaviors could be achieved by the magnetic machines. For instance, a variety of agile movements are developed for magnetic robots with fruitful inspirations from multilegged animals, zebrafish larvae, midge larvae, scallops, and jellyfish [10, 39–42]. Moreover, advanced functionalities including self-adaptation, shape memory, logic circuits, and mechanical tunability are achieved by the integration of magnetic control properties with structural designs and intelligent materials. Encoded with heterogeneous 3D magnetization profiles, magnetic robots could exhibit multiple complex deformations, e.g. 2D-to-3D and 3D-to-3D structural changes, upon magnetic stimulation. The arrangement of heterogeneous magnetization inside robotic structures is extensively studied, such as with the assistance of photolithography, modular assembly using bonding agents or dynamic covalent bonds, template-assisted magnetic programming, 3D printing techniques, and laser heating [16, 24, 27, 43–47]. In addition, the magnetothermal effect that could remotely generate heat using high-frequency magnetic fields is also developed for the activation of magnetic soft robots.

1.2.2 Light Actuation

Light is another commonly adopted actuation source for untethered miniature soft robots with the advantages of high spatial and temporal resolutions, enabling the precise and selective control [48]. Sophisticated optical equipment including photomasks, optical choppers, and lenses have been developed for the precise light actuation (Figure 1.1e,f). For instance, a single material component of LCE in cilia shape developed by Li et al. could present diverse complex deformation

behaviors including photophobic, phototropic motions, bending, and twisting using tunable light source [49]. The photo-responsive properties of soft robots could adapt to a wide spectrum or selective wavelength based on the optical absorptive and chemical properties of the material components. Photothermal effect and photochemical reactions are widely adopted as the working mechanisms for the synthetic light-responsive actuators. For example, through photonic–thermal energy conversion or photoisomerization of azobenzene derivatives, the ordering change in liquid crystal networks is often activated. A variety of other mechanisms including water desorption, change of surface tension, hydrophobicity, and magnetic properties, inequivalent thermal strain, and shape memory effect are also developed for the actuation of light-responsive materials [33, 50, 51]. For photo-responsive actuators, a two-layer structure design including an active layer and a passive layer has been widely adopted. The bending deformation of the bimorph actuators can be calculated according to the Timoshenko theory [50]:

$$\rho = \frac{(h_1 + h_2)\left[3(1+m)^2 + (1+mn)\left(m^2 + \frac{1}{mn}\right)\right]}{6(Le_2 - Le_1)(1+m)^2} \tag{1.4}$$

$$m = \frac{h_1}{h_2} \tag{1.5}$$

$$n = \frac{E_1}{E_2} \tag{1.6}$$

ρ represents the curvature radius. h_i and E_i ($i = 1, 2$) are the thickness and elastic modulus of the materials, respectively. Le_i ($i = 1, 2$) represent the expansion or shrinkage of the materials.

1.2.3 Acoustic Actuation

Acoustic actuation owns a wide range of applications in miniature robots and biomedical fields due to its good environmental adaptability and deep penetration into biological tissues [52, 53]. Acoustic radiation force and bubble assistance vibration have been developed for acoustic-actuated microrobots (Figure 1.1c,d).

The acoustic radiation force (F_A) applied to microrobots and the resonance frequency of a microbubble (f_{re}) can be obtained by Eqs. (1.7) and (1.8), respectively [54].

$$F_A = \oint_{\partial\Omega} \langle\sigma\rangle \cdot n \, dA - \oint_{\partial\Omega} \rho\langle v_1 v_2\rangle \cdot n \, dA \tag{1.7}$$

$$f_{re} \approx \frac{1}{2\pi}\sqrt{\frac{3\pi\kappa P_0}{8RL\rho}} \tag{1.8}$$

Ω is the surface of the microrobot. σ is the stress applied to the microrobot's surface and $\langle\sigma\rangle$ represents the time averaging value of σ. ρ and n refer to fluid density and the normal direction of the microrobot surface, respectively. v_1 is the vibration velocity. v_2 is the streaming velocity. R represents the bubble's radius and L represents the cavity's length. P_0 and κ are the hydrostatic liquid pressure and adiabatic index, respectively.

Mechanical resonance generated by integrated oscillatory units, e.g. sharp structures or bubbles in robot body, is needed to efficiently transform acoustic energy into mechanical energy and produce propulsion. Activated by acoustic energy, diverse locomotion modes including rotation, sliding movement, vertical climbing, starfish larvae-like motions, and pull-type motions have been achieved for microrobots [11, 53, 55]. A large thrust force can be generated via bubble assistance vibration in liquid environment even upon a low-amplitude acoustic field, while this type of actuation would be limited by the long-term stability of bubble. In comparison, the vibration of flexible structures is free from the long-term stability problem, but requires the input of high acoustic energy. One of the important properties of acoustic actuation is selective activation based on the design of robotic structures with well-separated resonance frequencies. To generate precise acoustic fields, strategies including time-lapse Fourier synthetic harmonics, acoustic holography methods, and phased-array acoustic waves have been proposed [56, 57].

1.2.4 Thermal Actuation

Thermo-responsive soft materials can be actuated by the change of environmental temperature in liquids or air (Figure 1.1h). However, at the small-scale size, the direct conversion of thermal energy to robots is relatively difficult. Strategies including electrical heating, electromagnetic heating, and photothermal conversion have been developed for miniature robots made of temperature-responsive materials, e.g. SMP, LCE, and poly(*N*-isopropylacrylamide) (PNIPAAm) hydrogel [58]. To generate heterogeneous deformation or execute target functions with better output performance, diverse methods have been proposed including the integration of materials with distinct thermal response behaviors, anisotropic alignment or patterning of thermal-responsive units, the optimization of robotic structures, and the pre-treatment of the thermal-responsive robots [59, 60]. For instance, soft robots that could exhibit self-oscillating behaviors upon temperature gradient generated by a hot plate were developed by Wang et al. and Dong et al. [32, 33]. Through the optimization of robotic structures, the thermal-responsive robots could achieve continuous crawling and rolling locomotion on the hot plate.

1.2.5 Chemical Actuation

Stimuli-responsive soft materials can also be actuated by other environmental stimuli including Marangoni effect (Figure 1.1g), humidity, chemical fuels, and ionic strength [54]. Chemical reactions that could generate bubbles have been widely adopted to propel miniature robots. The volumetric swelling or deswelling behaviors of water-absorbing materials have been exploited for hygroscopic robots to achieve programmable shape-morphing and movements (Figure 1.1i,j). Made of smart materials, soft robots could also exhibit responsive behaviors to the variations in pH, ionic strength, selective DNA sequences, surface tension gradient, and the presence of solvent or solvent vapor [61, 62]. Due to the advantages of ease in downscaling and wireless control, these robots could present high mobility and